

Preparation of MnO₂ modified magnetic graphitic carbon nitride composite and its adsorption toward Pb(II) in waste water

Wenning Xia and Yaochi Liu 

College of Chemistry and Chemical Engineering, Central South University, Changsha 410083, China

*Corresponding author. E-mail: liuyaochi72@163.com

ABSTRACT

Based on graphitic carbon nitride (CN) nanosheets, a novel MnO₂ modified magnetic graphitic carbon nitride composite (MMCN) was prepared via magnetization and in-situ deposition of MnO₂. Then, an array of characterizations and experiments were conducted to explore the physical and chemical properties of the synthesized MMCN material. The adsorption behavior and removal mechanism of the MMCN were also discussed intensively. The best pH value of Pb(II) of MMCN was 6. The maximum adsorption capacity of MMCN was as high as 187.6 mg/g, which was much higher than that of MCN and original CN, and removal percentage of Pb(II) was about 99%. The adsorption kinetics and isotherms were in accordance with the pseudo-second-order model and Langmuir model, respectively. The chemical adsorption of Pb(II) indicated that MMCN was a successful modified sorbent and pretty efficient to remove Pb(II) in an aqueous medium owing to the complexation and ion exchange of ample amino and hydroxyl groups. Moreover, MMCN could be separated easily from the aqueous medium under an external field after reaction with its magnetic performance.

Key words: adsorption, graphitic carbon nitride, magnetic, MnO₂, Pb(II)

HIGHLIGHTS

- A novel MnO₂ modified magnetic graphitic carbon nitride composite (MMCN) was prepared.
- The maximum adsorption capacity of MMCN toward Pb(II) was 187.6 mg/g and removal percentage of Pb(II) was around 99%.
- Characterization and batch experiments were conducted to investigate adsorption mechanism.
- The MMCN was a successful modified adsorbent and efficient to remove Pb(II) in aqueous medium.

INTRODUCTION

As one of the most critical resources, water is of enough significance for all creatures. However, much industrial and municipal waste water frequently contains various metal ions and this seriously exceeds the natural degradation capacity of ecology, having a fatal effect on the whole environment (Xu *et al.* 2018). Especially, Pb(II), a common heavy metal ion applied widely in the manufacturing field, can induce neurophysical disorders in children, even with a lead content in blood below 10 µg/dL (Uberoi & Shadman 1990; Safruk *et al.* 2017). The adsorption method, which is simple and inexpensive, has been considered as a promising approach to address the issue (Bailey *et al.* 1999; Ngah *et al.* 2011; Uddin 2017).

Among the alternative materials, graphitized carbon nitride (CN) has been considered as a promising material in research. The basic skeleton of CN is a kind of poly (3-S-triazine) rich in nitrification defects. The s-triazine ring of CN is a conjugated 2-D polymer structure and easy to form a p-conjugated planar layer (Amiri *et al.* 2016), which offers an excellent chemical and thermal stability. Noticing that the basic functional groups of the CN surface are mainly amino groups, they can bring numerous binding sites and capture Pb(II) quickly and accurately by complexation and ion-exchanged behavior (Zou *et al.* 2016). However, the original CN can only offer limited reactive sites, and it is difficult to separate from waste water owing to its high dispersion. Researches have shown that the introduction of some compatible materials is an effective method to conquer the conundrum (Guo *et al.* 2019a).

Herein, manganese dioxide (MnO₂) modified magnetic graphitic carbon nitride composite (MMCN) was prepared via in-situ deposition and applied in solution for Pb(II) removal. MnO₂ is chosen as the potential to add into the CN material for the remediation of lead cations. MnO₂ is a transition metal oxide with advantages of low-cost, good stability, and environmental compatibility (Moghaddam & Pakizeh 2015; Xiong *et al.* 2018).

This is an Open Access article distributed under the terms of the Creative Commons Attribution Licence (CC BY 4.0), which permits copying, adaptation and redistribution, provided the original work is properly cited (<http://creativecommons.org/licenses/by/4.0/>).

Especially, MnO_2 possesses a point of zero charge of ca.2.0 and has a large surface area with ample $-\text{OH}$ groups (Murray 1975; Gheju *et al.* 2016; Zhao *et al.* 2016), which can provide numerous active sites for $\text{Pb}(\text{II})$ in a wide range of $\text{pH} > 2.0$. Moreover, ferroferric oxide (Fe_3O_4) is also chosen as a modifier added to CN material because of its excellent performance separating from solution with an external electric field (Rajput *et al.* 2016; Zhou *et al.* 2018; Li *et al.* 2019).

MATERIALS AND METHODS

Materials

MMCN and MCN were prepared from analytical-reagent grade melamine ($\text{C}_3\text{N}_3(\text{NH}_2)_3$), manganese sulfate monohydrate ($\text{MnSO}_4 \cdot \text{H}_2\text{O}$), ferric chloride (FeCl_3) and ferrous sulfate heptahydrate ($\text{FeSO}_4 \cdot 7\text{H}_2\text{O}$). Lead source was confirmed as nitrate ($\text{Pb}(\text{NO}_3)_2$). They were obtained from Tianjin Kermel and Sinopharm. Potassium permanganate (KMnO_4) and the remaining materials were purchased in Macklin. All water used in the experiment was purified deionized water.

Methods

The obtained adsorbent was characterized by a variety of techniques. Scanning electron microscopy (SEM, VEGA3SBH, CZE) was used to determine the morphology of samples. The surface functional groups of samples were determined by Fourier transform infrared spectrometer (FTIR, Nicolet 6700, USA). Powder X-ray Diffraction (XRD) specimen samples were characterized by Bruker Advance D8 diffractograph with Cu ($\text{K}\alpha$) radiation. The surface chemistry of MMCN and the adsorbed MMCN samples were determined using X-ray photoelectron spectroscopy (XPS, Escalab 250, USA). The specific surface area and porosity of samples were analyzed at 77 K by Brunauer-Emmett-Teller (BET, JW-BK132F, China). At room temperature, the potential changes of MMCN samples were detected using the Zeta potential analyzer (DELSA 440SX, USA). Vibration sample magnetometer (VSM, MPMS XL-7, USA) tested the magnetic properties of MMCN samples. And properties of MMCN composite for $\text{Pb}(\text{II})$ adsorption was evaluated by the experimental studies. Removal mechanism of the adsorbents were also confirmed to evaluate the application of $\text{Pb}(\text{II})$ on MMCN.

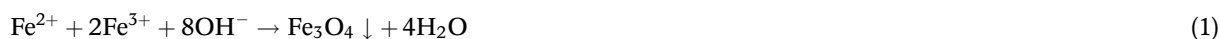
Preparation of materials

Preparation of CN, MCN and MMCN

Through the typical pyrolysis method (Guo *et al.* 2019a), CN was prepared in following steps. 12 g of melamine powder was put in a coppel and roasted at 550°C for 3 h in atmosphere. After cooling up the faint yellow bulk to room temperature, it was washed with water and ethanol for times and dried it at 323 K for 24 h, and ground the bulk into powder for spare finally.

The MCN composite was synthesized through in-situ deposition of Fe_3O_4 particles on the surface of CN. The detailed procedures are described as follows. Under an atmosphere of nitrogen, 1.00 g as-preparation CN, 1.20 g $\text{FeSO}_4 \cdot 7\text{H}_2\text{O}$ and 2.32 g $\text{FeCl}_3 \cdot 6\text{H}_2\text{O}$ were mixed in 80 ml deionized water and the mixture was stirred for 30 min. Then $\text{NH}_3 \cdot \text{H}_2\text{O}$ solution (30%, v/v) was added in drops until the pH value of aqueous was 10.0. The suspension continued to be stirred for 2 h at 353 K. After filtering, washing and drying the products, the black solids were collected by a magnet.

The MMCN composite was prepared by the following steps. 1 g as-prepared MCN and 1.17 g $\text{MnSO}_4 \cdot \text{H}_2\text{O}$ were mixed in 80 ml deionized water stirring for 0.5 h at room temperature. Then the mixture was heated to 353 K and 0.5 g KMnO_4 granules added into it slowly. The whole reaction system was kept agitating for 5 h to obtain MMCN composite. Finally, the black composite was washed with distilled water and ethanol, respectively. The preparation process of MMCN can be described by the diagram in Figure 1. The synthetic mechanisms of Fe_3O_4 and MnO_2 nanoparticles are expressed as follows:



Adsorption properties

Batch of sorption experiments was displayed to optimize the correlative factor of MMCN material for $\text{Pb}(\text{II})$ adsorption. The values of adsorption capacity were calculated by ultraviolet spectrophotometer according to

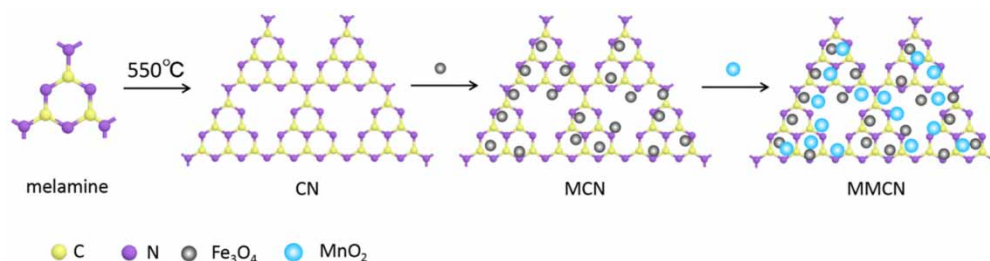


Figure 1 | The diagram of the MMCN preparation.

colorimetric theory (Resano *et al.* 2019). Therefore, the adsorption quantity of MMCN for Pb(II) was calculated by Equation (3):

$$Q_e = (C_o - C_e) \times \frac{V}{m} \quad (3)$$

(1) Different adsorbents and dosage:

CN, MCN and MMCN were conducted here as the adsorbent for Pb(II), 0.02 g adsorbent was added into a conical flask contained 40 mL Pb(II) solution (50 mg/L). To study the effect of dose, MMCN dosages of 0.25–2 g/L were added 40 mL Pb(II) solution at 100 mg/L.

(2) Effect of pH value on adsorption:

The pH of the solution was adjusted by 0.1 mol/L HNO₃ and 0.1 mol/L NaOH solutions to 2, 3, 4, 5, 6, 7, 8, respectively. and 0.02 g MMCN was added into a conical flask with a Pb(II) concentration of 100 mg/L. The pH of the solution was the solution was vibrated for 270 min at 298 K and 170 r/min. The concentration of Pb(II) in the supernatant after adsorption equilibrium was measured and calculated by ultraviolet spectrophotometry. Each sample was repeated at least 3 times.

(3) Adsorption kinetics:

The effect of contact time between 0 and 270 min of Pb(II) on different adsorbents were investigated at 298 K, and the initial concentration of the Pb(II) solution was 30, 100, 250 mg/L and the pH was 6.0. The concentration of Pb(II) in the supernatant was measured and calculated at different contact time.

(4) Adsorption isotherms:

The adsorption isotherm of Pb(II) on MMCN was studied at 298, 308 and 318 K. 0.02 g MMCN were added to 40 mL Pb(II) solution at concentration of 20–180 mg/L for 270 min at 170 r/min, respectively. After adsorption equilibrium, the concentration of Pb(II) in the supernatant was measured and calculated.

RESULTS AND DISCUSSION

Characterizations of materials

The surface morphology of CN, MCN and MMCN were observed by SEM. As shown in Figure 2, CN had an aggregated, layered and irregular plate-like structure, which was consistent with the reported literature (Guo *et al.* 2019b). Differently from the smooth surface of CN, the MCN was composed of many bulk particles and possessed a non-smooth surface morphology. Clearly, many nanoparticles were found on the surface of MMCN, which could be due to the appearance of MnO₂ on the outer surface of MCN. As for the EDS elemental mapping of MCN and MMCN, the Fe and Mn were uniformly distributed in the synthesized MCN and MMCN material, which proved the mass deposition of Fe₃O₄ on CN, MnO₂ in MMCN and the successful modification of CN.

To further understand the microstructures of CN, MCN and MMCN, the BET characterization of the two materials was studied and is shown in Figure 3 and Table 1, which implied a IV type isotherm and a H4 type hysteresis loop according to the classification of IUPAC, meaning a mixture of microporous and mesoporous adsorbent. Obviously, the surface area of MMCN (262.78 m²/g) was much larger than that of MCN (16.45 m²/g) and the original CN (5.47 m²/g). MMCN pores were mainly distributed within the mesoporous range with centered pore diameter of 4.89 nm. Generally speaking, higher specific surface area offered more

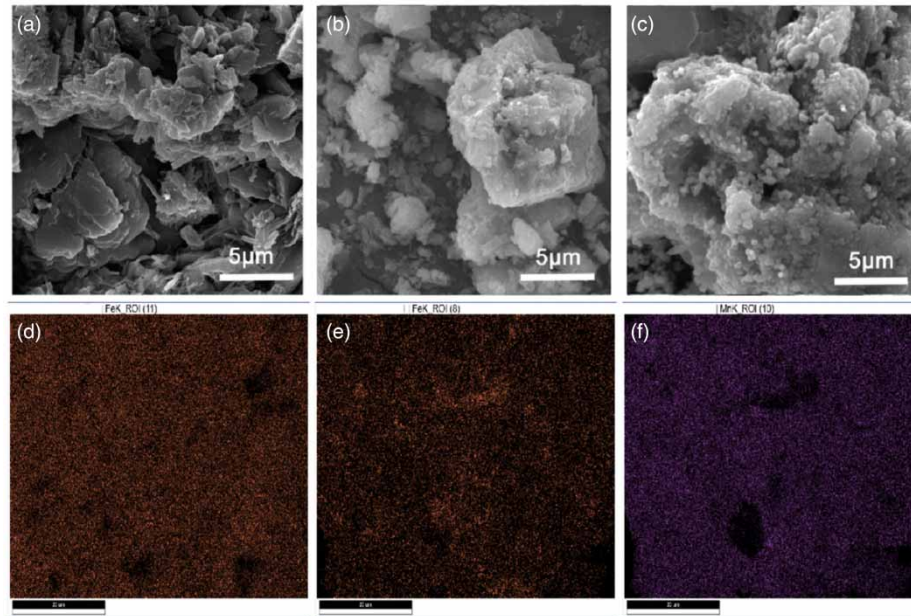


Figure 2 | SEM images of (a) CN, (b) MCN and (c) MMCN; EDS elemental mapping images of (d) Fe in MCN, (e) Fe in MMCN, (f) Mn in MMCN.

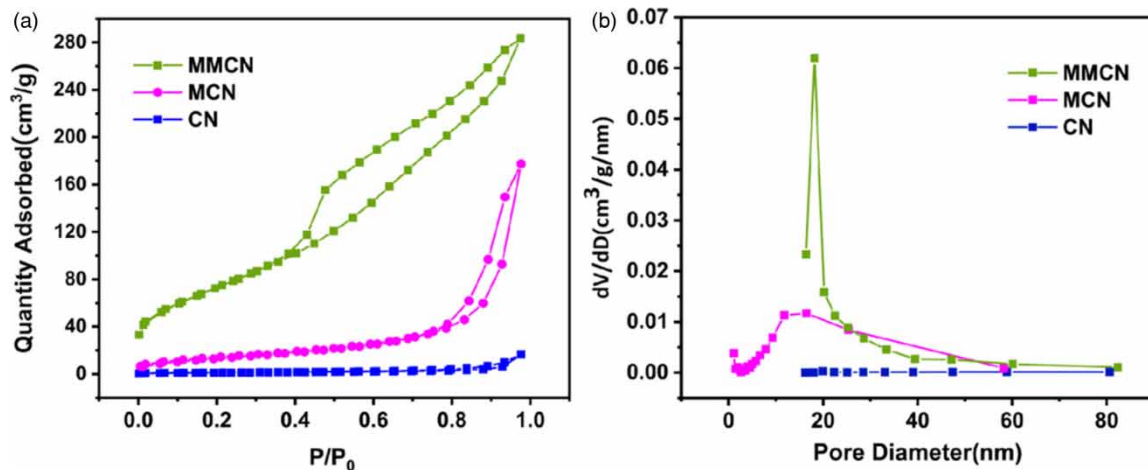


Figure 3 | (a) The BET isotherms of CN, MCN and MMCN; (b) The pore size distribution curves of CN, MCN and MMCN.

Table 1 | Pore structure properties of CN, MCN and MMCN

Material	BET surface area (m²/g)	BJH pore volume (cm³/g)	BJH pore diameter (nm)
CN	5.47	0.026	39.94
MCN	16.45	0.283	16.45
MMCN	262.78	0.443	4.89

sorption sites for Pb(II) (Li *et al.* 2018a). The corresponding pore size distribution plots suggested the MMCN composite had more pores than single CN, which could provide an interchange channel for adsorption. The increased surface area and numerous mesopores would be momentous to the sorption process.

The FTIR spectra of CN, MCN and MMCN are presented in Figure 4(a) as the importance of functional groups in sorption. The characteristic peak at 806 cm⁻¹, which belonged to the triazine units of CN, was observed in the spectra of all adsorbents and several peaks in the range of 1,100 and 1,700 cm⁻¹ were the typical stretching vibrations of tri-s-triazine derivatives (Tian *et al.* 2016), which indicated that MCN and MMCN

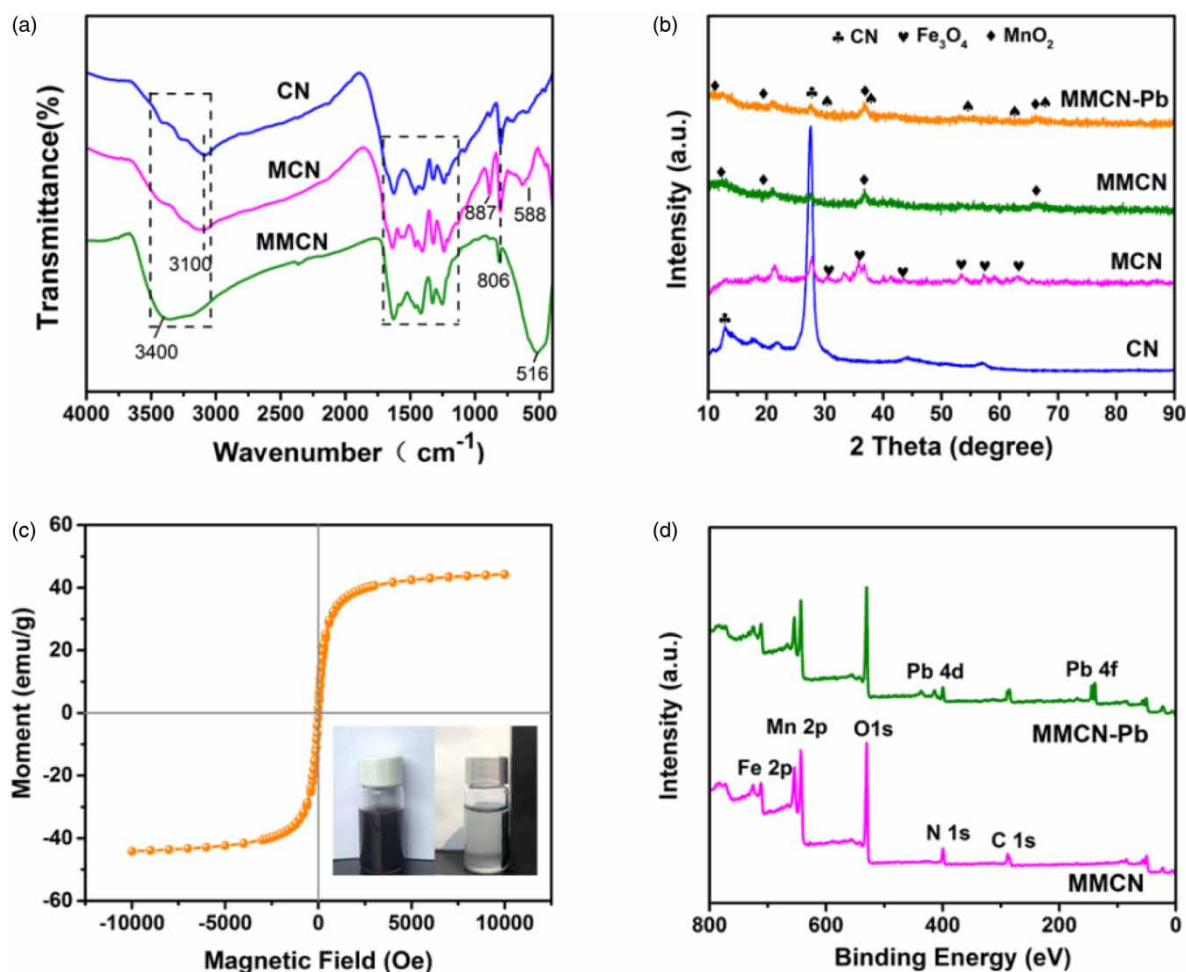


Figure 4 | (a) FTIR spectra of CN, MCN and MMCN; (b) X-ray diffraction patterns of CN, MCN, MMCN and MMCN-Pb; (c) VSM curve of MMCN (the inset is the photo of magnetic separation); (d) XPS full-scan spectra of MMCN and MMCN-Pb composite.

retained the structure of tri-s-triazine in CN after modification. The significant band at ca. 588 cm^{-1} in the FTIR spectrum of MCN could be assigned to Fe-O (Shi *et al.* 2018), signalling the formation of Fe_3O_4 on the CN. For MMCN, a new peak was observed at 516 cm^{-1} , which was due to the stretching of the Mn-O bond (Dubal *et al.* 2011). Moreover, the broad peak at $3,000\text{--}3,500\text{ cm}^{-1}$ mainly represented the stretching vibration behavior of amino ($-\text{NH}$ and $-\text{NH}_2$) and $-\text{OH}$ groups (Tian *et al.* 2016; Zhang *et al.* 2019). Noticing the band at $3,000\text{--}3,500\text{ cm}^{-1}$, the central peak of MMCN had a significant shift compared to that of MCN and CN, which suggested enhancement of hydrogen band interaction owing to the appearance of more functional groups (Zhou *et al.* 2017). The results illustrated that magnetization and modification had been conducted successfully and the process occurred probably through chemical deposition.

The XRD patterns of the CN, MCN, MMCN and MMCN-Pb composite are presented in Figure 4(b). The strong peaks at 13.0° (100) and 27.5° (002) in the XRD spectra of CN indicated an excellent crystallinity. The typical peaks of CN were also observed in the other three materials, which illustrated the structural stability of CN. The characteristic peaks of MCN at $2\theta = 30.5^\circ$ (220), 35.9° (311), 43.6° (400), 53.5° (422), 57.4° (511), and 63.0° (440) were attributed to the typical crystal faces of Fe_3O_4 (Chen *et al.* 2019). As for MMCN, the peaks at 12.3° , 18.6° , 36.9° and 65.7° (PDF 18-0802) belonging to MnO_2 were found in the spectra, which could be attributed to the cover of mass MnO_2 on the surface of MCN and the characteristic peaks of Fe_3O_4 were more obscure than before. The results were fully consistent with that of FTIR. In the XRD pattern of MMCN-Pb composite, some weak but noteworthy peaks were found at 32° , 36.8° , 52.7° , 62.6° and 65.6° (PDF 03-1156), which suggested the presence of Pb in crystal character and successful adsorption of lead onto MMCN.

Magnetic responsivity was a conspicuous characteristic of magnetic materials. Figure 4(c) shows the magnetic hysteresis loop of MMCN and the saturation magnetization value of 44 emu/g , implying that the MMCN composite

could be isolated from aqueous medium easily after adsorption by an external ordinary magnet, just as expressed in the inset picture. The loop of MMCN was without any hysteresis and symmetrical about the origin, which meant that the superparamagnetism of MMCN could meet the demand of magnetic separation from aqueous medium. The MMCN material, with excellent separation property, provided a sustainable site for the remediation of heavy metal.

The XPS survey spectra of MMCN and MMCN-Pb composite are shown in Figure 4(d). We could see Pb 4d and Pb 4f peaks in the XPS survey of MMCN-Pb while not appearing in that of MMCN, which indicated the existence of divalent Pb on the surface of MMCN after loading (Xu *et al.* 2013). The spectrum of Pb 4f in Figure 5(f) exhibited that two characteristic peaks at 143.4 and 138.5 eV were assigned to Pb 4f_{5/2} and Pb 4f_{7/2}, respectively.

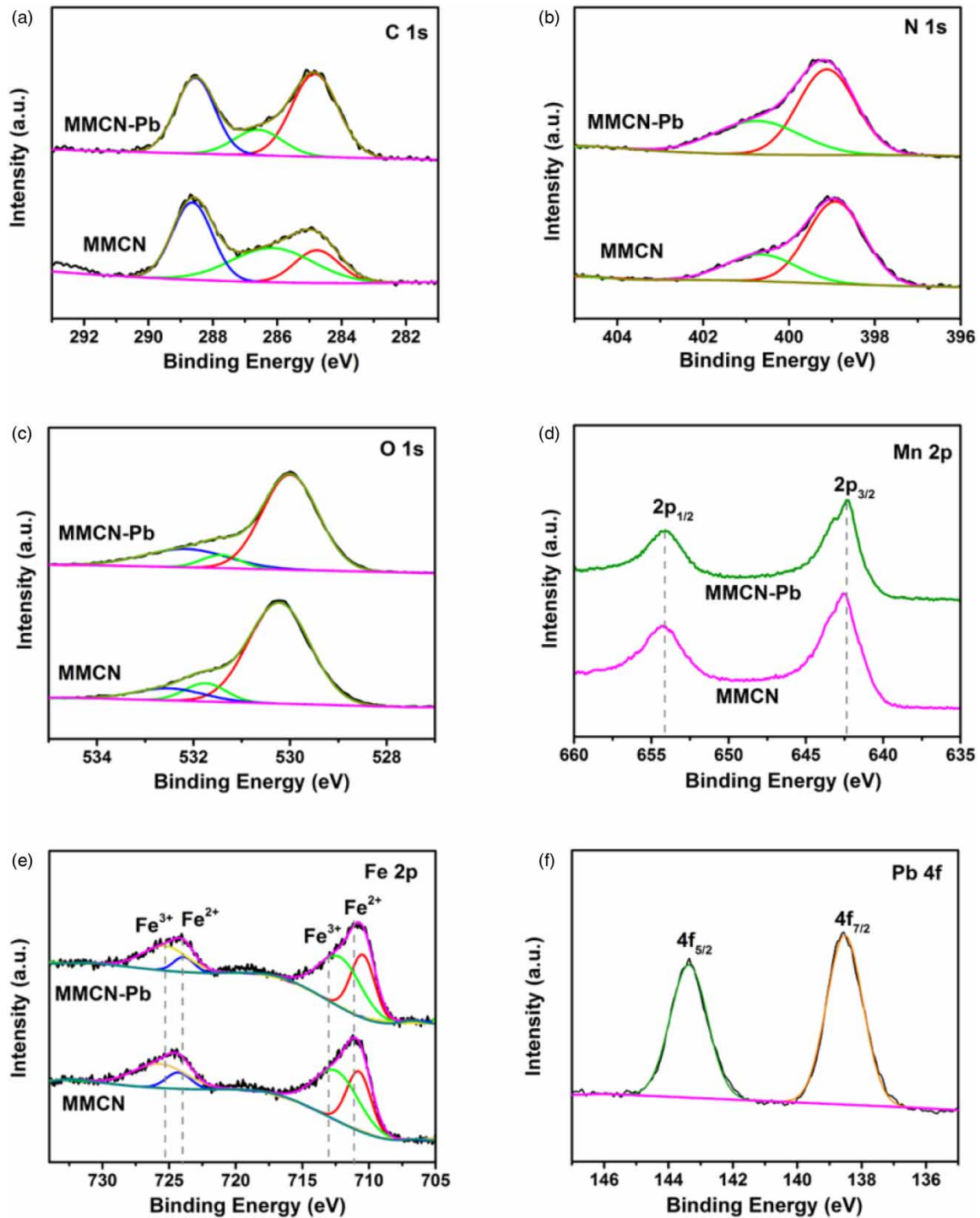


Figure. 5 | XPS high resolution spectra of (a) C 1s, (b) N 1s, (c) O 1s, (d) Mn 2p, (e) Fe 2p, and (f) Pb 4f.

Two peaks at 654.3 and 642.5 eV for Mn 2p^{1/2} and Mn 2p^{3/2} (Figure 5(d)) spin – orbit suggested the chemical state of Mn as Mn (IV) (Li *et al.* 2018b), while the weak shift of the peak after adsorption was due to the interruption of Pb(II) (Liang *et al.* 2017). From the XPS result of Fe 2p in Figure 5(e), the calculated Fe²⁺/Fe³⁺ ratios of the MMCN before and after adsorption were around 0.5, which indicated the existence of Fe₃O₄ in composite (Zhao *et al.* 2016). As shown in Figure 5(a), three intense peaks were identified at ca. 288.6/288.5 eV, 286.2/286.7 eV and 284.7/284.9 eV, which correspond to the sp² C-N bond, C-O bond and the sp² hybrid carbon on the N-containing aromatic ring N = C-N, respectively (Wu *et al.* 2019). The XPS spectra of N 1s (Figure 5(b)) could be divided into two peaks at around 399.0 eV and 401.0 eV, the N 1s binding energy of MMCN-Pb showed an obviously higher peak than that of MMCN, which could be attributed to the coordination of N with Pb (Li *et al.* 2018a). Meanwhile, the O 1s (Figure 5(c)) peaks in MMCN material exhibited a contrary change after load of Pb(II), indicating an interactive effect between MMCN and lead. There was a peak at ca.530 eV in the high resolution of O 1s, which could be attributed to Fe-O-Fe and Mn-O-Mn (Zhao *et al.* 2016). The ratio of the integral area of the surface hydroxyl oxygen (ca. 531 eV) to the total oxygen decreased from 9.64% to 6.92% after Pb(II) adsorption, indicating that the surface hydroxyl was related to the Pb(II) adsorption process (López-Muñoz *et al.* 2016). In conclusion, the adsorption force of Pb (II) on MMCN is a chemical process and mainly related to ample hydroxyl and amino groups on the exterior of MMCN.

Effect of adsorbent dosage and pH

A series of experiments about the effect factors including different adsorbents, adsorbent dosage and initial pH in aqueous medium on the Pb(II) removal were conducted and the data are exhibited in Figure 6. In Figure 6(a), the capacity of MMCN to Pb(II) was as high as 127.19 mg/g, which was much higher than that of CN and MCN, showing an excellent effect of modification. Distinctly in Figure 6(b), with the increasing dosage of MMCN

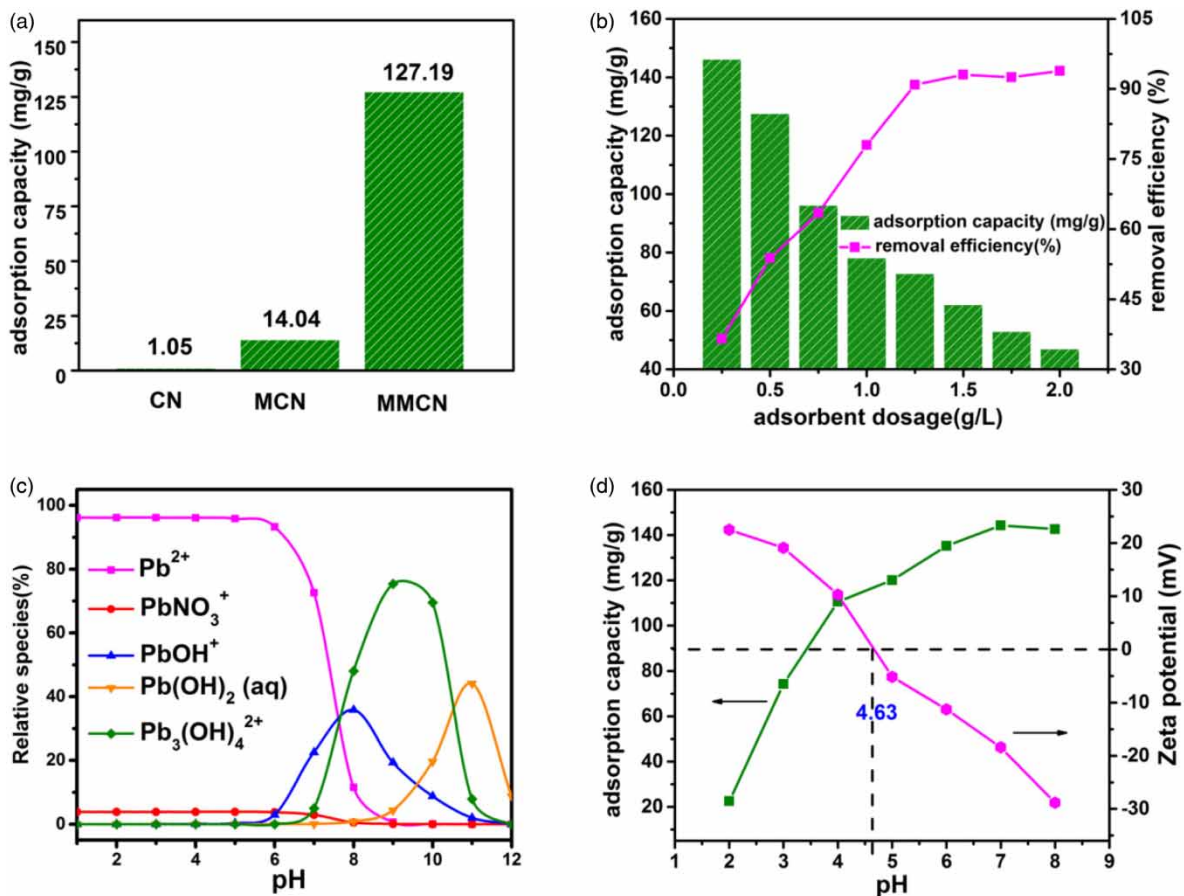


Figure 6 | (a) Adsorption capacity of CN, MCN, and MMCN for Pb(II); (b) effect of MMCN dosage on Pb(II) removal; (c) relative species of lead at various pH calculated by Visual MINTEQ (ver.3.0.); (d) the zeta potential of MMCN and the effect of pH for Pb(II) removal on MMCN.

from 0.25 to 2.0 g/L, the removal percentage of Pb(II) increased gradually and stabilized at around 99%. Instead, the adsorption capacity negatively correlated with MMCN content. Considering to the experimental loss, the optimal dosage of MMCN was 1.0 g/L.

pH value is another effective factor of adsorption capacity, as shown in Figure 4(d). In the pH range of 2–8, the capacity rose sharply when $\text{pH} < 4$, increased slowly at pH 4–6 and finally reached a plateau at 6–8. The phenomenon could be explained by the surface charge of MMCN and the species distribution of Pb in aqueous medium. The pH_{PZC} of the MMCN was confirmed at around 4.63. When $\text{pH} < 4$, lower than pH_{PZC} , the positive charge of MMCN induced by protonation would bring electrostatic repulsion between MMCN and Pb(II) and the ample H^+ would compete with Pb(II) to unite with negative groups on the surface MMCN. With the pH value increasing, the electrostatic repulsion became weaker and Pb(II) became the dominant species of lead when the pH was lower than 6. As the pH value continued to grow, the lead started to precipitate based on the species distribution of lead obtained from Visual MINTEQ (ver.3.0.). Considering all above results, pH = 6 was chosen as the optimum pH.

Adsorption kinetics study

A bunch of experiments were carried out to study the effect of initial concentration and contact time on MMCN adsorption for Pb(II). From data in Figure 7(a), the adsorption quantity of MMCN rose rapidly in the first 20 min and the rate slowed down 50 min later. Finally, the adsorption equilibrium was approached at around 90 min. The higher rate at the start was relevant to the higher concentration of Pb(II) and the existence of abundant active sites, which indicated that chemical adsorption occurred primarily in the process. In order to further study the practical application of the sorption, the pseudo-first-order and pseudo-second-order models were chosen to simulate the adsorption kinetic. Both of the linear fitting curves and correlative parameters are presented in Figure 7(b) and 7(c) and Table 2. As shown, the adsorption capacity worked out by the pseudo-second-order model was more relevant to the experimental converts compared with the former, and the correlation coefficient close to 1 suggested that the pseudo-second-order model was more satisfying to approach the actual adsorption kinetics. These results reflected that adsorption was really a chemical process which involved valence forces between adsorbents and metal ions (Liu *et al.* 2019).

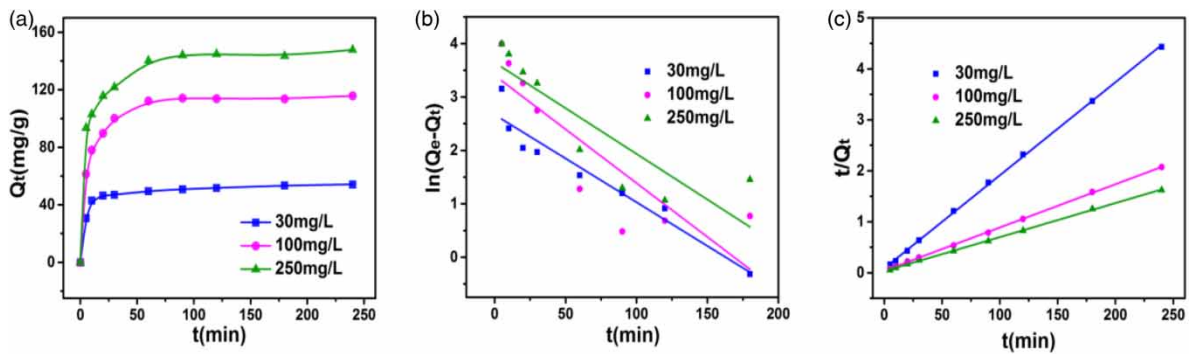


Figure 7 | (a) Effect of time on the removal process; fitting curves of (b) pseudo-first-order and (c) pseudo-second-order models.

Table 2 | Kinetic parameters of MMCN adsorption at different initial Pb(II) concentrations

C_0 (mg/L)	Q_{exp} (mg/g)	Pseudo-first-order			Pseudo-second-order		
		Q_{cal} (mg/g)	k_1 (min^{-1})	R^2	Q_{cal} (mg/g)	k_2 ($\text{min} \cdot \text{mg/g}$)	R^2
30	54.17	14.42	0.016	0.92	54.76	0.0038	0.9997
100	115.82	30.11	0.020	0.69	117.92	0.0018	0.9998
250	147.81	38.32	0.017	0.72	149.70	0.0014	0.9996

Q_{exp} , the adsorption quantity of MMCN from experiment.

Q_{cal} , the adsorption quantity of MMCN from calculation through fitting curve.

Isotherms and thermodynamic studies of reaction

The thermodynamic and isotherms of MMCN for Pb(II) at 298, 308, and 318 K are exhibited in Figure 8. Obviously, the highest adsorption capacity of Pb(II) onto MMCN occurred at 318 K and Q_m here was 187.6 mg/g, which showed higher temperature was favorable for the adsorption process. Then these isotherm data were demonstrated by Langmuir and Freundlich models as follows.

$$\text{Langmuir model } \frac{C_e}{Q_e} = \frac{1}{k_L Q_m} + \frac{C_e}{Q_m} \quad (4)$$

$$\text{Freundlich model } \ln Q_e = \ln k_f + \frac{1}{n} \ln C_e \quad (5)$$

where Q_e (mg/g) and Q_m (mg/g) mean equilibrium adsorption capacity and the maximum theoretical monolayer capacity of MMCN, respectively; C_e (mg/L) is the concentration of Pb(II) at equilibrium; k_L (L/mg), k_f (mg/g) and n represent the Langmuir affinity, Freundlich constant and the intensity of adsorption, respectively.

From Table 3, the correlation coefficient of the Langmuir model was clearly higher than that of the Freundlich, implying the former was more appropriate to describe the Pb(II) removal on MMCN. Therefore, the adsorption behavior seemed to be conducted on a homogeneous surface in a monolayer according to the fundamental assumptions of the Langmuir model. In addition, a dimensionless separation factor (R_L) was introduced to

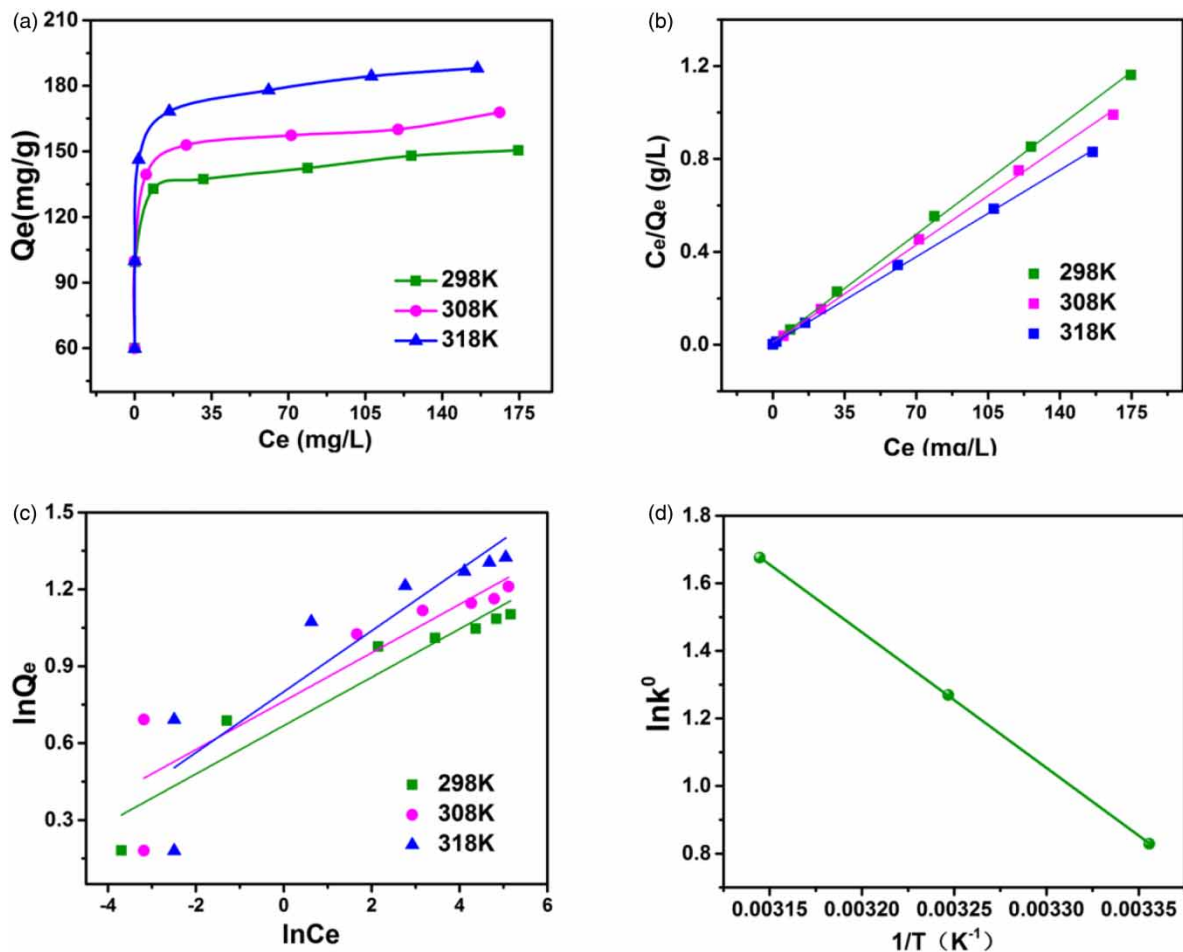


Figure 8 | (a) Sorption isotherms of MMCN for Pb(II); linear plots of (b) Langmuir and (c) Freundlich isotherms; (d) linear correlation relationship of $\ln k^0$ and $1/T$.

Table 3 | Correlative isotherm parameters of MMCN for Pb(II) at different temperatures

T (K)	Langmuir isotherm				Freundlich isotherm	
	Q _m (mg/g)	k _L (L/mg)	R ²	R _L	k _f (mg/g)	R ²
298	150.2	0.704	0.9992	0.006–0.045	1.95	0.8992
308	165.8	0.758	0.9986	0.005–0.042	2.15	0.7853
318	187.6	0.974	0.9995	0.004–0.033	2.23	0.7844

judge whether the above characteristics of the Langmuir simulation were credible or not. The R_L was expressed as:

$$R_L = \frac{1}{1 + k_L C_0} \quad (6)$$

The value of R_L can be used to reveal the feasibility of the reaction. There are four situations: one of them is 0 < R_L < 1, which means favorable; and the bigger the R_L, the better for the removal. From what is shown in Table 3, the obtained R_L values implied the adsorption of Pb(II) on MMCN was favorable.

To evaluate the thermodynamic characteristics of the MMCN composite, the related thermodynamic parameters (i.e., ΔG⁰, ΔH⁰ and ΔS⁰) were studied as follows. The thermodynamic equations can be represented as:

$$\ln(K^0) = \frac{\Delta S^0}{R} - \frac{\Delta H^0}{RT} \quad (7)$$

$$\Delta G^0 = -RT \ln K^0 \quad (8)$$

where K⁰ is the equilibrium coefficient of sorption. ΔG⁰, ΔH⁰ and ΔS⁰ mean the standard free energy, enthalpy change and entropy change, respectively. They can be calculated by the slope and y-intercept in a Van't Hoff plot (Li *et al.* 2018a). The calculated negative values of ΔG⁰ indicated that the high temperature was conducive to the spontaneous adsorption process of Pb(II) on MMCN. Meanwhile, the positive values of ΔH⁰ and ΔS⁰ demonstrated a natural endothermic reaction with increasing randomness and it agreed with the above fact of higher adsorption capacity at higher temperature.

Here is a comparison of adsorption conditions and capacity of different adsorbent agents with that in the work. From the data in Table 4, it is clear to see a better effect of the MMCN than other previous adsorbents in similar studies. So, the MMCN adsorption is an effective and promising method to remove Pb(II) from aqueous medium.

Table 4 | Comparison with recent similar studies

Adsorbents	pH	T(K)	Adsorption capacity(mg/g)	References
FAAS	6.0	/	32.48	Lu <i>et al.</i> (2016)
SDAC	6.5–8.0	303 ± 2	46.70	Sreejalekshmi <i>et al.</i> (2009)
White pottery clay	5.5	293	159.24	Li <i>et al.</i> (2020)
MWCNTs	5.0	298	91.00	Wang <i>et al.</i> (2007)
Pb(II)-IIP	/	298	33.15	Ao & Guan (2017)
Pb-ICB	/	303	177.62	Jing <i>et al.</i> (2016)
MMCN	6.0	318	187.6	This work

CONCLUSION

A new adsorbent named MMCN for Pb(II) was prepared via magnetization and in-situ deposition of MnO₂. An array of characterizations and experiments were conducted to explore the synthesized MMCN material and removal behavior toward Pb(II). The adsorption kinetics, thermodynamics and removal mechanisms of the

MMCN were also analyzed. The maximum adsorption capacity of MMCN for Pb(II) was as high as 187.6 mg/g, which was much higher than that of the original CN, and removal percentage of Pb(II) was around 99%. These results indicated that MMCN was pretty efficient to remove Pb(II) in aqueous medium by complexation and ion exchange with ample amino and hydroxyl. Moreover, MMCN could be separated easily under an external field after reaction because of its magnetic performance.

ACKNOWLEDGEMENTS

This study was supported by the Postgraduate Independent Exploration and Innovation Project of Central South University, China (No. 206021711) and the Key Research and Development Project of Hunan Province, China (No. 2019KW2031).

CONFLICT OF INTEREST

The authors declare that they have no conflict of interests.

DATA AVAILABILITY STATEMENT

All relevant data are included in the paper or its Supplementary Information.

REFERENCES

- Amiri, M., Salehniya, H. & Habibi-Yangjeh, A. 2016 Graphitic carbon nitride/chitosan composite for adsorption and electrochemical determination of mercury in real samples. *Ind. Eng. Chem. Res.* **55**, 8114–8122.
- Ao, X. & Guan, H. 2017 Preparation of Pb(II) ion-imprinted polymers and their application in selective removal from wastewater. *Adsorpt. Sci. Technol.* **36**(5), 774–787.
- Bailey, S., Olin, T., Bricka, R. & Adrian, D. 1999 A review of potentially low-cost sorbents for heavy metals. *Water Res.* **33**, 2469–2479.
- Chen, B., Chen, S., Zhao, H., Liu, Y., Long, F. & Pan, X. 2019 A versatile β -cyclodextrin and polyethyleneimine bi-functionalized magnetic nanoadsorbent for simultaneous capture of methyl orange and Pb (II) from complex wastewater. *Chemosphere* **216**, 605–616.
- Dubal, D. P., Dhawale, D. S., Gujar, T. P. & Lokhande, C. D. 2011 Effect of different modes of electrodeposition on supercapacitive properties of MnO_2 thin films. *Appl. Surf. Sci.* **257**, 3378–3382.
- Gheju, M., Balcu, I. & Mosoarca, G. 2016 Removal of Cr (VI) from aqueous solutions by adsorption on MnO_2 . *J. Hazard. Mater.* **310**, 270–277.
- Guo, J., Chen, T., Zhou, X., Zheng, T., Xia, W., Zhong, C. & Liu, Y. 2019a Preparation and Pb (II) adsorption in aqueous of 2D/2D g- $\text{C}_3\text{N}_4/\text{MnO}_2$ composite. *Appl. Organomet. Chem.* **33**, e5119.
- Guo, Y., Wang, Y., Zhao, S., Liu, Z., Chang, H. & Zhao, X. 2019b Photocatalytic oxidation of free cyanide over graphitic carbon nitride nanosheets under visible light. *Chem. Eng. J.* **369**, 553–562.
- Jing, Y., Yin, N. & Yu, X. 2016 Pb(II)-imprinted chitosan beads to enhance the adsorption property and selectivity: characterization, kinetics, and thermodynamics. *Desalin. Water Treat.* **57**(32), 15073–15082.
- Li, X., Xing, J., Zhang, C., Han, B., Zhang, Y., Wen, T., Ieng, R., Jiang, Z., Ai, Y. & Wang, X. 2018a Adsorption of lead on sulfur-doped graphitic carbon nitride nanosheets: experimental and theoretical calculation study. *ACS Sustainable Chem. Eng.* **6**, 10606–10615.
- Li, Y., Zhao, R., Chao, S., Sun, B., Wang, C. & Li, X. 2018b Polydopamine coating assisted synthesis of MnO_2 loaded inorganic/organic composite electrospun fiber adsorbent for efficient removal of Pb^{2+} from water. *Chem. Eng. J.* **344**, 277–289.
- Li, M., Wei, D., Liu, T., Liu, Y., Yan, L., Wei, Q., Du, B. & Xu, W. 2019 EDTA functionalized magnetic biochar for Pb (II) removal: adsorption performance, mechanism and SVM model prediction. *Sep. Purif. Technol.* **227**, 115696.
- Li, G., Zhang, J., Liu, J., Sun, C. & Yan, Z. 2020 Adsorption characteristics of white pottery clay towards Pb(II), Cu(II), and Cd(II). *Arabian J. Geosci.* **13**(13), 519.
- Liang, J., Li, X., Yu, Z., Zeng, G., Luo, Y., Jiang, L., Yang, Z., Qian, Y. & Wu, H. 2017 Amorphous MnO_2 modified biochar derived from aerobically composted swine manure for adsorption of Pb(II) and Cd(II). *ACS Sustainable Chem. Eng.* **5**, 5049–5058.
- Liu, J., Chen, Y., Han, T., Cheng, M., Zhang, W., Long, J. & Fu, X. 2019 A biomimetic SiO_2 @chitosan composite as highly-efficient adsorbent for removing heavy metal ions in drinking water. *Chemosphere* **214**, 738–742.
- López-Muñoz, M. J., Arencibia, A., Cerro, L., Pascual, R. & Melgar, Á. 2016 Adsorption of Hg(II) from aqueous solutions using TiO_2 and titanate nanotube adsorbents. *Appl. Surf. Sci.* **367**, 91–100.
- Lu, X. H., Zhao, M. Q., Li, P. J. & Nurulla, I. 2016 Adsorption behavior of Pb(II) ion imprinted magnetic composite adsorbent in aqueous solution by FAAS. *Spectroscopy Spectral Anal.* **36**(5), 1483–1487.
- Moghaddam, H. & Pakizeh, M. 2015 Experimental study on mercury ions removal from aqueous solution by MnO_2/CNTs nanocomposite adsorbent. *J. Ind. Eng. Chem.* **21**, 221–229.

- Murray, J. 1975 The interaction of metal ions at the manganese dioxide-solution interface. *Geochim. Cosmochim. Acta* **39**, 505–519.
- Ngah, W., Teong, L. & Hanafiah, M. 2011 Adsorption of dyes and heavy metal ions by chitosan composites: a review. *Carbohydr. Polym.* **83**, 1446–1456.
- Rajput, S., Pittman Jr., C. & Mohan, D. 2016 Magnetic magnetite (Fe_3O_4) nanoparticle synthesis and applications for lead (Pb^{2+}) and chromium (Cr^{6+}) removal from water. *J. Colloid Interface. Sci.* **468**, 334–346.
- Resano, M., García-Ruiz, E., Aramendía, M. & Belarra, M. A. 2019 Quo vadis high-resolution continuum source atomic/molecular absorption spectrometry. *J. Anal. At. Spectrom.* **34**(1), 59–80.
- Safarik, A., McGregor, E., Aslund, M., Cheung, P., Pinsent, C., Jackson, B. & Sigal, E. A. 2017 The influence of lead content in drinking water, household dust, soil, and paint on blood lead levels of children in Flin Flon, Manitoba and Creighton, Saskatchewan. *Sci. Total Environ.* **593**, 202–210.
- Shi, S., Yang, J., Liang, S., Li, M., Gan, Q., Xiao, K. & Hu, J. 2018 Enhanced Cr (VI) removal from acidic solutions using biochar modified by $\text{Fe}_3\text{O}_4/\text{SiO}_2\text{-NH}_2$ particles. *Sci. Total Environ.* **628**, 499–508.
- Sreejalekshmi, K. G., Krishnan, K. A. & Anirudhan, T. S. 2009 Adsorption of Pb(II) and Pb(II)-citric acid on sawdust activated carbon: kinetic and equilibrium isotherm studies. *J. Hazard. Mater.* **161**(2–3), 1506–1513.
- Tian, J., Zhang, L., Fan, X., Zhou, Y., Wang, M., Cheng, R., Li, M., Kan, X., Jin, X., Liu, Z., Gao, Y. & Shi, J. 2016 A post-grafting strategy to modify g- C_3N_4 with aromatic heterocycles for enhanced photocatalytic activity. *J. Mater. Chem. A* **4**, 13814–13821.
- Uberoi, M. & Shadman, F. 1990 Sorbents for removal of lead compounds from hot flue gases. *AIChE. J.* **36**, 307–309.
- Uddin, M. 2017 A review on the adsorption of heavy metals by clay minerals, with special focus on the past decade. *Chem. Eng. J.* **308**, 438–462.
- Wang, H., Zhou, A., Feng, P., Yu, H. & Yang, J. 2007 Mechanism study on adsorption of acidified multiwalled carbon nanotubes to Pb(ii). *J. Colloid Interface Sci.* **316**(2), 277–283.
- Wu, B., Li, Y., Su, K., Tan, L., Liu, X., Cui, Z., Yang, X., Liang, Y., Li, Z., Zhu, S., Yeung, W. & Wu, S. 2019 The enhanced photocatalytic properties of $\text{MnO}_2/\text{g-C}_3\text{N}_4$ heterostructure for rapid sterilization under visible light. *J. Hazard. Mater.* **377**, 227–236.
- Xiong, X., Ji, Y., Xie, M., You, C., Yang, L., Liu, Z., Asirid, A. & Sun, X. 2018 $\text{MnO}_2\text{-CoP}_3$ nanowires array: an efficient electrocatalyst for alkaline oxygen evolution reaction with enhanced activity. *Electrochem. Commun.* **86**, 161–165.
- Xu, M., Wang, H., Lei, D., Qu, D., Zhai, Y. & Wang, Y. 2013 Removal of Pb (II) from aqueous solution by hydrous manganese dioxide: adsorption behavior and mechanism. *J. Environ. Sci.* **25**, 479–486.
- Xu, J., Cao, Z., Zhang, Y., Yuan, Z., Lou, Z., Xu, X. & Wang, X. 2018 A review of functionalized carbon nanotubes and graphene for heavy metal adsorption from water: preparation, application, and mechanism. *Chemosphere* **195**, 351–364.
- Zhang, L., Fu, F. & Tang, B. 2019 Adsorption and redox conversion behaviors of Cr (VI) on goethite/carbon microspheres and akaganeite/carbon microspheres composites. *Chem. Eng. J.* **356**, 151–160.
- Zhao, J., Liu, J., Li, N., Wang, W., Nan, J., Zhao, Z. & Cui, F. 2016 Highly efficient removal of bivalent heavy metals from aqueous systems by magnetic porous $\text{Fe}_3\text{O}_4\text{-MnO}_2$: adsorption behavior and process study. *Chem. Eng. J.* **304**, 737–746.
- Zhou, J., Liu, Y., Zhou, X., Ren, J. & Zhong, C. 2017 Removal of mercury ions from aqueous solution by thiourea-functionalized magnetic biosorbent: preparation and mechanism study. *J. Colloid Interf. Sci.* **507**, 107–118.
- Zhou, X., Zhou, J., Liu, Y., Guo, J., Ren, J. & Zhou, F. 2018 Preparation of iminodiacetic acid-modified magnetic biochar by carbonization, magnetization and functional modification for Cd (II) removal in water. *Fuel* **233**, 469–479.
- Zou, Y., Wang, X., Ai, Y., Liu, Y., Ji, Y., Wang, H., Hayat, T., Alsaedi, A., Hu, W. & Wang, X. 2016 β -Cyclodextrin modified graphitic carbon nitride for the removal of pollutants from aqueous solution: experimental and theoretical calculation study. *J. Mater. Chem. A* **4**, 14170–14179.

First received 17 January 2021; accepted in revised form 17 June 2021. Available online 30 June 2021